Initial Condition Dependene of Dynamis and Evaporation of Polymer Spallation Partiles Flying in Polymer Ablated Arcs

doi: 10.1109/ICEPE-ST.2015.7368325

Initial Condition Dependence of Dynamics and Evaporation of Polymer Spallation Particles Flying in Polymer Ablated Arcs

Takuya Nakagawa[1], Tomoyuki Nakano[1], Yasunori Tanaka[1], Yoshihiko Uesugi[1], Tatsuo Ishijima[1]
[1]Kanazawa University, Kakuma, Kanazawa 920-1192, Japan

***Abstract*— We have developed a numerical model on dynamics of spallation particles flying in the polymer ablated arcs. We had found microsized " spallation particles" ejected from polyamide materials (Polyamide-6 (PA6) $[-C_6H_{11}ON-]_n$/Polyamide 66 (PA66) $[-C_{12}H_{22}O_2N_2-]_n$) by thermal plasma contact. In this paper, effects of initial conditions for spallation particles flying in polymer ablated arcs on dynamics and evaporation of polymer spallation particles were investigated using the developed numerical model. As initial conditions, pressure inside the polymer ablated arc, the initial particle diameter and initial velocity of spallation particles were treated to study their effects. Under the given temperature and gas flow distributions in specified initial conditions, the trajectories of spallation particles flying in the polymer ablated arc were simulated numerically, considering the time variations in the temperature and the diameter of the particles. The results show that the highest flight altitude of the PA6 spallation particle flying in the PA6 ablated arc is affected by the initial particle diameter and velocity remarkably.**

***Index Terms*— Circuit breaker, Current interruption, Ablation, Spallation, Polyamide**

I. Introduction

Polymer materials are widely used for quenching chamber walls or for dielectric insulation in molded case circuit breakers (MCCB) in a low-voltage electric distribution system. The polymer materials contact intensive arc plasmas during a short-circuit fault or a ground fault, and this contact induces ablation of the polymer materials. The polymer ablation vapor causes a large pressure rise in the arc quenching chamber. This induces gas flow and convection loss in the arc plasma. The produced gas flow forces to expand the arc plasma, and helps cooling down and quenching it. In this way, Such polymer ablation remarkably affects the interruption capability of the circuit breakers [1]. It also affects the thermodynamics and transport properties of arc quenching medium. Circuit breakers applying the polymer ablation are widely developed and used [2]. However, the interaction between arc plasmas and arc quenching polymer mediums has not revealed in detail.

In our previous work, we had observed not only polymer ablation vapor but also micro-sized particles "spallation particles" ejected from polyamide materials during the irradiation of inductively coupled thermal plasmas (ICTPs) [3]. We call this phenomenon "spallation phenomenon". It had been also founded that the spallation phenomenon can be enhanced remarkably due to water absorption for polyamide materials [4]. In this case, the thermodynamics and transport properties of PA6 ablation vapor hardly changed due to its water absorption. This is attributed to the fact that the composition of PA6 ablation vapor originally contains H and O atoms composed by water. If the spallation phenomenon applys for the arc quenching, spallation particles are expected to penetrate into the arc core, which can cool down it directly. Therefore, such application of spallation phenomenon for arc quenching lead to enhance the arc interrupiton capability of the circuit breaker. For this aim, it is necessary to understand dynamics of the particles in the arc plasma.

In this paper, a numerical model for a spallation particle motion and temperature increase was used. Firstly, temperature and gas flow distributions in the PA6 ablated arc were calculated using a numerical thermo-fluid model [5], [6], [7]. Effects of PA6 ablation vapor on the arc plasma such as the change in the thermodynamics and transport properties of arc medium, the energy loss due to the ablation, the mass exchange and the pressure rise due to the produced gas flow in the arc plasma were considered. Under those computed distributions in the PA6 ablated arc, we simulated the motion and temperature variations of PA6 spallation particles having an initial velocity and a particle diameter solving the equation of motion and the mass and energy conservation equation [9]. Through this simulation, we could understand the trajectory and temperature variation of the particle including its phase change and a decrease in its particle diameter. Not only initial parameters of PA6 particles such as its initial velocity, particle diameter and ejection position but also the initial pressure in the PA6 ablated arc were varied respectively in the present work. From the results, we could understand the condition in which PA6 particles can ablate in the arc core. The Results indicated that the highest flight altitude of PA6 spallation particles flying in the PA6 ablated arc is affected by the initial velocity and particle diameter remarkably.

II. Numerical thermo-fluid analysis of polymer ablated arc

For the simulation in the motion and the temperature variation of PA6 spallation particles flying in the PA6 ablated arc, we had to calculate its temperature and gas flow distributions at first. Therefore, the numerical thermo-fluid analysis model to calculate those distributions is indicated in this section.

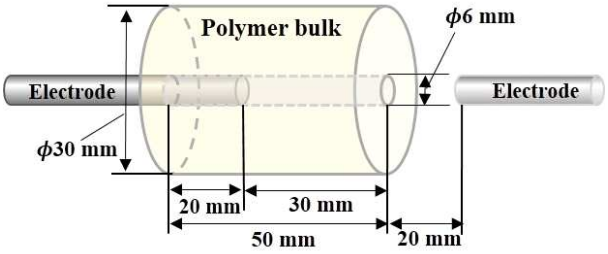

Fig. 1. Schematics of the calculation target imaging the arc device.

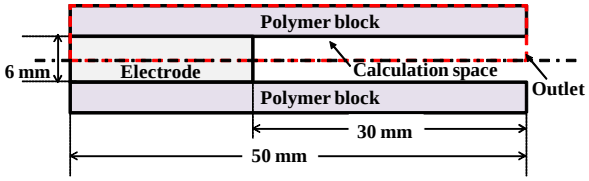

Fig. 2. Calculation space for the temperature and gas flow distributions in the polymer ablated arc.

TABLE I

CALCULATION CONDITIONS FOR THE STEADY-STATE ANALYSIS OF THE TEMPERATURE AND GAS FLOW DISTRIBUTIONS IN THE PA6 ABLATED ARC.

Current value	DC 50 A
Length between the electrodes	50 mm
Arc quenching polymer medium	PA6
Electrode material	Fe

TABLE II

THERMODYNAMIC PROPERTIES OF PA6

Melting temperature [K]	493.5
Thermal decomposition temperature [K]	717.6
Latent heat for melting [kJ/kg]	53.3
Latent heat for thermal decomposition [kJ/kg]	187.6
Mass density [kg/m^3]	1140
Specific heat in solid [J/(kg K)]	2617
Specific heat in liquid [J/(kg K)]	3031
Thermal conductivity [W/(m K)]	0.25
Emissivity of the surface	0.3

A. Assumptions

Fig. 1 shows the calculation target imaging the arc device in this model. In the calculation target, two cylindrical electrodes are located with a distance of 50 mm. Each of elecrode has a diameter of 6 mm. One of the electrodes is inserted in the cylindrical polymer material. On the other hand, A length of the polymer cylinder is 50 mm. In addition, its inner diameter is 6 mm, and its external diameter is 30 mm. In this simulation, the arc plasma ignites between the electrodes. The arc ignition space is filled with air at first. The contact between the arc plasma and the cylindrical polymer material causes the polymer ablation.Fig. 2 shows the calculation space in this model. The calculation space is the cross section of the cylindrically symmetrical space with the electrode and the cylinderical polymer shown as a broken line colored in red in Fig. 2. It is divided into 104 grids in an axial direction, and into 42 grids in a radial direction.

In calculating, the following assumptions are defined: (i) the plasma is in local thermodynamic equilibrium; consequently, all relevant temperatures such as the electron temperature, the gas temperature and the excitation temperature are mutually identical. (ii) the plasma is in optically thin for wavelengths greater than 200 nm. For wavelengths of less than 200 nm, 20% of the total emission coefficient is accounted for radiation loss to consider the effective light absorption. (iii) the flow is steady, laminar and axisymmetric, with negligible viscous dissipation. (iv) the calculation space is the symmetrical space. (v) the electric field generates only in the axial direction. (vi) the propagation velocity of pressure waves is limited. (vii) the phenomena such as melting and boiling of the electrode materials, the electrode fall voltage and the process of electron emission are neglected.

B. Governing equation

On the assumptions shown in section II-A, the polymer ablated arc is considered to be governing by the mass conservation equation, the momentum equation, the energy conservation and the mass conservation equation of polymer ablation vapor. These equations are mentioned in another paper [8].

In this computation, the mass production rate due to ablation S_{p}^{C} was approximately calculated only for the neighbor to the polymer wall[8]. The ablation flux Γ_{ab} used for calculating it was computed by the Hertz-Knudsen relation [8]. On the other hand, the deposition flux Γ_{dep} was evaluated by the random flux [8].

C. Calculation conditions

The calculation conditions are summarized in Table. I. In this calculation, the current value was set to DC 50 A. The cylindrical polymer material was defined to be made of PA6. The electrode material was Fe. The thermodynamic properties of PA6 required in this calculation is summarized in Table. II.

D. Calculation results

The calculated two dimensional temperature and gas flow distributions in the PA6 ablated arc at DC 50 A is shown in Fig. 3. From Fig. 3 the temperature on the axis is higher than those near the polymer inner wall. On the other hand, the gas flow velocity become higher toward the gas outlet.

Fig. 4(a) shows the radial temeperature distributions at each axial position of $z = 30$ mm and $z = 50$ mm in the PA6 ablated arc. As seen, the temperature on the axis reach above 11000 K. On the other hand, the regions near the inner polymer wall is cooled by the PA6 ablation vapor, and the temperature there become lower than 1000 K. The produced PA6 ablation vapor makes the arc shrinking in the radial direction

The radial gas flow velocity distributions at each axial position of $z = 30$ mm and $z = 50$ mm in the PA6 ablated arc are shown in Fig. 4. From Fig. 4 the gas flow velocity on the gas outlet $z = 50$ mm is higher than that

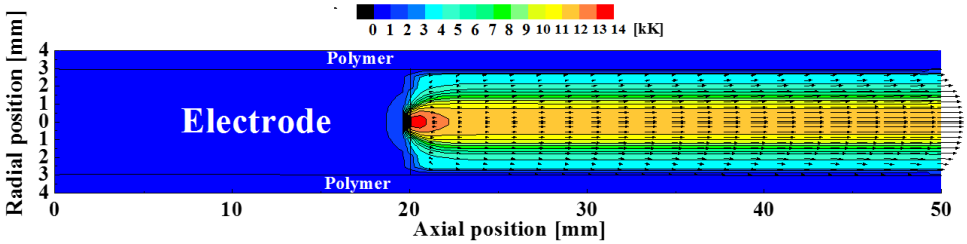

Fig. 3. Calculated two dimensional temperature and gas flow distributions in the PA6 ablated arc.

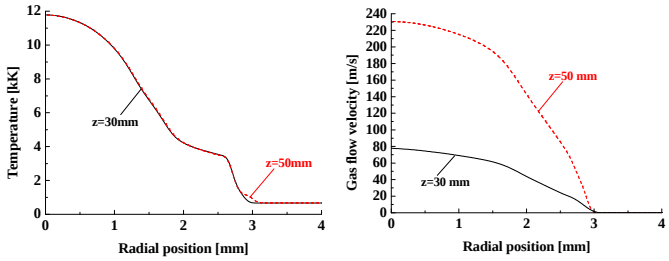

(a) Temperature (b) Gas flow velocity

Fig. 4. Radial temperature and gas flow velocity distributions in the PA6 ablated arc.

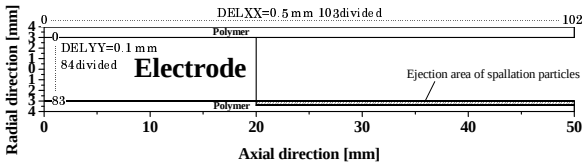

Fig. 5. Calculation space for the simulation on dynamics and the temperature variation of spallation particles flying in the PA6 ablated arc.

at $z = 30$ mm. The ejected PA6 ablation vapor induces such difference.

III. Simulation on Dynamics and Temperature Variation of Spallation Particles Ejected in the PA6 Ablated Arc

A. Calculation space for simulation on dynamics and temperature variation of spallation particles

Fig. 5 shows the calculation space for the simulation on dynamics and the temperature variation of spallation particles flying in the PA6 ablated arc. This simulation uses the temperature and gas flow distributions in the PA6 ablated arc calculated in the previous section. The calculation space is devided into 103 grids in an axial direction and 84 grids in a radial direction respectively. Spallation particles are ejected from the lower wall of the cylindrical polymer material shown in Fig. 5.

B. Model of spallation particle

1) Momentum equation of spallation particles ejected in the polymer ablated arc: In this calculation, spallation particles were assumed to be completely spherical. It was also assumed that the motion of spallation particles flying in the arc plasma are affected only by the drag force from the viscosity of the arc and by the gravity. The image and the definition of each parameter in the motion of spallation particle show in Fig. 6. On those assumptions, the momentum equation for a particle exposed to the polymer ablated arc can be written as[12]

$$\frac{du_\mathrm{p}}{dt} = -\frac{3}{4} C_\mathrm{D} \left(u_\mathrm{p} - u\right) U_\mathrm{R} \left(\frac{\rho}{\rho_\mathrm{p} d_\mathrm{p}}\right) + g \tag{1}$$

$$\frac{dv_\mathrm{p}}{dt} = -\frac{3}{4} C_\mathrm{D} \left(v_\mathrm{p} - u\right) U_\mathrm{R} \left(\frac{\rho}{\rho_\mathrm{p} d_\mathrm{p}}\right) \tag{2}$$

$$U_\mathrm{R} = \sqrt{\left(u_\mathrm{p} - u\right)^2 + \left(v_\mathrm{p} - v\right)^2} \tag{3}$$

$$C_\mathrm{D} = \begin{cases} \frac{24}{Re} & Re \leq 0.2 \\ \frac{24}{Re}\left(1 + \frac{3}{16} Re\right) & 0.2 < Re \leq 2.0 \\ \frac{24}{Re}\left(1 + 0.11 Re^{0.81}\right) & 2.0 < Re \leq 21.0 \\ \frac{24}{Re}\left(1 + 0.189 Re^{0.62}\right) & 21.0 < Re \leq 200 \end{cases} \tag{4}$$

$$Re = \frac{\rho U_\mathrm{R} d_\mathrm{p}}{\mu} \tag{5}$$

where U_R is the relative velocity between the particle and the arc plasma, C_D is the drag coefficient, g is the gravitational acceleration, u_p is the axial velocity of the particle, v_p is the radial velocity of the particle, u is the axial velocity of ablation vapor, v is the radial velocity of ablation vapor, ρ_p is the mass density of the particle in solid and liquid phases, ρ is the mass density of ablation vapor, d_p is the particle diameter, μ is the viscosity of ablation vapor, Re is Reynolds number. Reynolds number in this computation was typically in range of 0 - 13.1.

2) Energy conservation equation and mass conservation equation of spallation particle: The temperature inside the spallation particle can be non-uniform due to its lower thermal conductivity. Therefore, the temperature distribution can be produced inside the paricle. To consider this temperature distribution, the particle was divided into 20 shells shown in Fig. 7. We define the temperature $T_\mathrm{p}(r,t)$ and the liquid fraction $\chi(r,t)$ of each shell, and these parameter depend on the radial position r and the time t. We also assumed that the

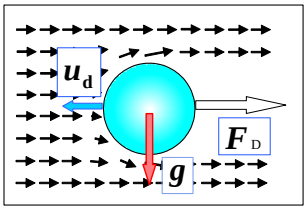

Fig. 6. Exerted drag force and gravity on a spallation particle flying in gas flow.

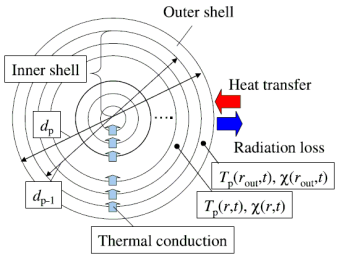

Fig. 7. Concept of a spallation particle treating its inner temperature gradient.

thermal decomposition of the particle occured when its temperature reached to T_e.

Inside the particle, thermal conduction between inner shells due to the radial temperature gradient was considered for any temperature range [8]. On the other hand, more complex phenomenon such as thermal conduction to the inner shells, heat transfer from the surrounding arc plasma, the radiation loss from the surface of the particle were considered at the outershell [8]. The temperature and the liquid fraction at the outer shell were calculated by the equations mentioned in another paper []. The decrease in the particle diameter due to its thermal decomposition was computed by the mass of its ablation [8].

C. Calculation condition

The calculation conditions of the spallation particle for the simulation were summarized in Table. III. We assumed that the PA6 particles ejected from the PA6 inner wall at the axial position of 30 mm and the radial position of 3 mm randomly. The initial temperature of the particle was set to 450 K corresponding to the temperature of the inner wall. Its initial velocity was set to 5 m/s due to its experimental measurement in the previous work [9]. In addition, we estimated the initial diameter to be 0.12-0.28 mm by the comparison between the experimental trajectories of the particles flying during the irradiation of ICTPs and its numerical trajectories in another calculation. From this work, the initial particle diameter was set to 0.2 mm in this simulation. We defined the angle α of the initial velocity shown in Fig. 8 and the angle α was set to $\pm 9°$, $\pm 27°$ and $\pm 45°$.

IV. Calculation results and discussion

Fig. 9 shows the trajectories of the PA6 particles ejected in the PA6 ablated arc. In Fig. 9, these trajectories are

TABLE III

Initial conditions of the spallation particle for the simulation of its dynamics and temperature variation in the PA6 ablated arc

Treated polymer material	PA6
Initial velocity of the particle [m/s]	5.0
Initial particle diameter of the particle [mm]	0.2
Initial temperature of the particle [K]	450
Initial ejecting position of the particle [mm]	(z,r)=(30,3)
Division number of the particle diameter	20

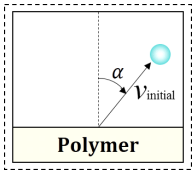

Fig. 8. Definition of an angle α of the initial velocity of a spallation particle.

shown lines colored with respective colors. For any angle α, the particle penetrates into the temperature region of about 7000 K to 9000 K and evaporates completely there. This may cool down the high temperature region which the PA6 ablation vapor can't do, and consequently the arc plasma is expected to be quenched effectively by the penetration of spallation particles.

In this calculation, the time variations in the temperature of each shell and the particle diameter were calculated for each angle α. These show in Fig. 10 for α=9° and α=27°. The time t is referred to the initiation of the particle ejection. At α=9°, the temperature in the outer shell increases due to the exposition to the arc plasma. Around t=15 μs, it reaches the melting temperature and keeps the temperature. This attributes to the fact that the energy which the particle is given by the arc is consumed for the latent heat for its melting. After that, the temperature increases again, and it reaches the thermal decomposition temperature at t=45 μs. The particle diameter decreases at the same time. The temperatures of the inner shells increase one after another after its completely thermal decomposition. The particle diameter decreases due to thermal decomposition of the shells, and the particle completely decomposes around t=400 μs. Such time variations in the temperature and the particle diameter can be seen similarly for every α. From these results, we can expect that the spallation phenomenon may lead to the rapidly arc quenching effect.

A. Initial condition dependence of dynamics and evaporation of polymer spallation particles

By using this model, we investigated the initial condition dependence of dynamics and evaporation of the PA6 particles ejected in the PA6 ablated arc. In present work, the initial velocity, the particle diameter and the ejection position of the particle and the initial pressure in the PA6 ablated arc were varied respectively. According to the change of these parameters, the variations in the highest flight altitude of the particles ejected were investigated.

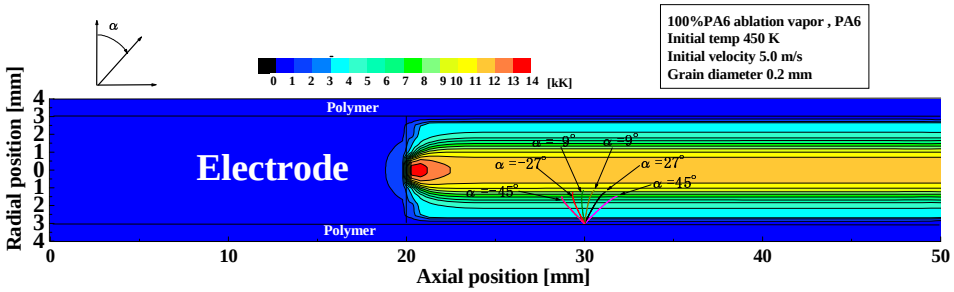

Fig. 9. Trajectories of the PA6 spallation particles ejected from the lower wall at the axial position of 30 mm in the PA6 ablated arc.

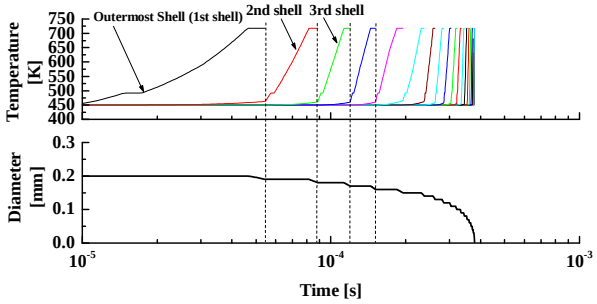

(a) α=9°

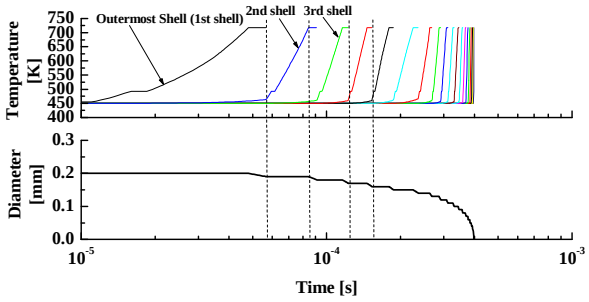

(b) α=27°

Fig. 10. Time variations in the temperature of each shell and the particle diameter for α=9° and α=27°

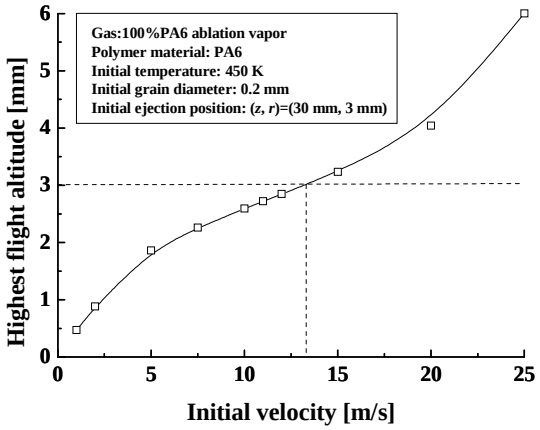

Fig. 11. Initial velocity dependence of the highest flight altitude of the particles ejected in the PA6 ablated arc.

Firstly, the initial velocity of the particle was changed from 1-25 m/s, and the other parameters were set to the same values summarized in Table. III. Fig. 11 shows the initial velocity dependence of the highest flight altitude of the particles flying in the PA6 ablated arc. As seen, the highest flight altitude of the particle depends on its initial velocity remarkably. The highest flight altitude increases with increasing its initial velocity.To decomposition and cool down the arc core, the particle may be required to have the initial velocity higher than 13 m/s.

Secondly, we changed the initial particle diameter 0.1-0.5 mm. The other values were fixed shown in Table. III. Fig. 12 shows the initial particle diameter dependence of the highest flight altitude of the particle ejected in the PA6 ablated arc. In Fig. 12, the highest flight altitude of the PA6 particle almost increases linearly as the increase of the particle diameter. The particle also needs to having the initial particle diameter of 0.32 mm to reach the arc core. Thus, the particle having an initial particle diameter less than 0.32 mm can not be expected to cool down the arc core effectively.

Next, the initial position from the particles ejected is varied 25 - 45 mm at the axial position. We set the other parameter to each value as shown in Table. III. The initial ejection position dependence of the particle ejected in the PA6 ablated arc is shown in Fig. 13. As seen, the highest flight altitude of the particle ejected from each position hardly changes. At any positions, the particles penetrate into the arc to the height of about 2 mm. Therefore, we can find to obtain the cooling effect given by the particles uniformly in the PA6 ablated arc.

Finally, we varied the initial pressure in the PA6 ablated arc 0.1 - 2.0 MPa. The parameters of the particle were set to the same values shown in Table. III. Fig. 14 shows the initial pressure dependence of the highest flight altitude of the particle ejected in the PA6 ablated arc. The highest flight altitude of the particle hardly changes with increasing the initial pressure in the PA6 ablated arc, and it almost keeps the constant value of about 1.8 mm. Thus, the increase of the initial pressure in the PA6 ablated arc is not expected to affect the dynamics and evaporation of the particle ejected in the PA6 ablated arc.

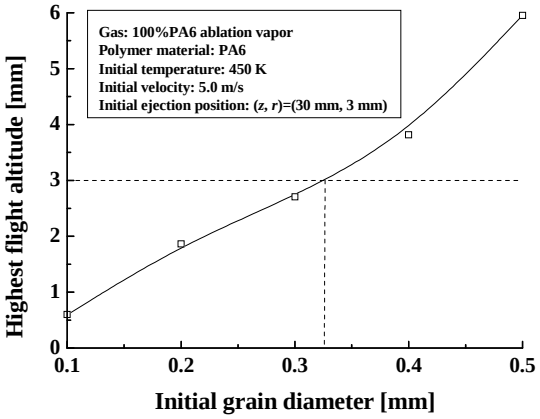

Fig. 12. Initial particle diameter dependence of the highest flight altitude of the particle ejected in the PA6 ablated arc.

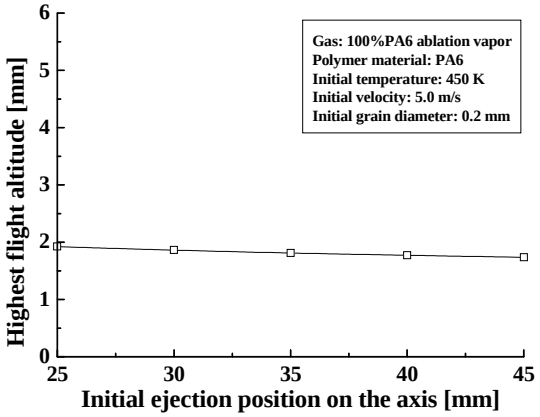

Fig. 13. Initial ejected position dependence of the highest flight altitude of the particle ejected in the PA6 ablated arc.

V. Summary

In this paper, the initial parameter dependence of the highest flight altitude of the PA6 spallation particle flying in the PA6 ablated arc was investigated using the numerical model in the dynamics and evaporation of the particle. For this aim, the temperature and gas flow distributions in the PA6 ablated arc were calculated at first. We computed the trajectories of the particles flying under those distributions in the PA6 ablated arc, considering the time variations in the temperature in each shell of the paricle and the particle diameter. This model also consider the temperature distribution inside the particle leading to melting and thermal decomposition of the particle. In this model, we varied the initial parameters of the particle such as its initial velocity, its particle diameter and its ejection position.The initial pressure in the PA6 ablated arc was also changed. The results indicate that the dynamics and evaporation of the particle can be affected remarkably by its initial velocity and particle diameter. On the other hand, the initial ejected position and the initial pressure hardly affects those. From these results, the arc quenching effect of the spallation phenomenon is expected to depend on the velocity and particle diameter of the spallation particle remarkably.

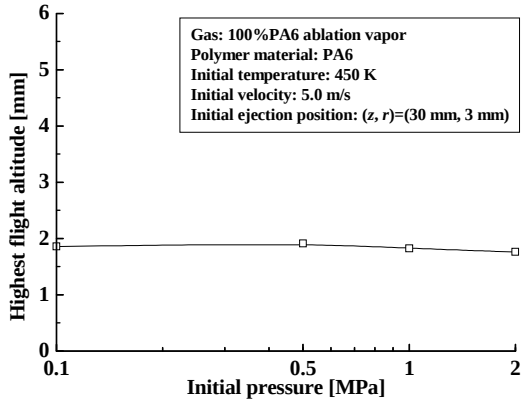

Fig. 14. Initial pressure dependence of the highest flight altitude of the ejected in the PA6 ablated arc.

References

[1] D. Eichhoff, A. Kurz, R. Kozakov, G. Gotto, D. Uhrlandt, A. Schnettler: "Study of an ablation-dominated arc in a model circuit breaker", *J. Phys. D: Appl. Phys.*, Vol.45, No.30, 305204 (2012)

[2] M. Tsukima, T. Mitsuhashi, M. Takahashi, M.Fushimi, S. Hosogai, S. Yamagata: "Low-voltage Circuit Breaker using Auto-puffer Interruption Technique", *IEEJ Trans.PE*, Vol.122, No.9, pp. 969-975 (2002) (in Japanese)

[3] Y. Tanaka, N. Shinsei, K. Amitani, Y. Uesugi, J. Wada, S. Okabe: "Spallation Particle Ejection From Polymer Surface Irradiated by Thermal Plasmas", *IEEE Trans. Plasma Sci*, Vol.39, No.11, pp. 2776-2777 (2011)

[4] N. Shinsei, M. Ishida, T. Tanaka, Y. Uesugi, T. Ishijima: "Ejection frequency of spallation particles from polyamide materials with water absorption irradiated by Ar thermal plasma with molecular gases", *Proc. Int. Workshop High Voltage Engineering 2012 (IWHV2012)*, ED-12-122, SP-12-050, HV-12-053 (2012)

[5] T. Onchi, Y. Tanaka, Y. Uesugi: "Effect of polymer ablation gas on arc quenching properties around current zero", *IEEJ Trans. PE*, Vol.131, No.7, pp. 609-620 (2011)

[6] T. Onchi, Y. Tanaka, K. Kawasaki, Y. Uesugi: "Thermofluid simulation of arc plasmas confined by a polymer hollow cylinder", *IEEJ Trans. PE*, Vol.131, No.2, pp. 196-204 (2011)

[7] H. Horikawa, Y. Tanaka, Y. Uesugi: "Numerical Simulation and Experiment on Decay of Polymer Ablation Arcs under Free Recovery Condition", *The Papers of Joint Technical Meeting on Electrical Discharges, Static Apparatus and Switching and Protecting Engineering, IEE Japan*, ED-11-065, SA-11-038, SP-11-011 (2011)

[8] T. Nakagawa, T. Nakano, Y. Tanaka, Y. Uesugi, T. Ishijima: "Numerical Simulation on Dynamics and Thermal Decomposition of Spallation Polymer Particles Flying in Polymer Ablated Arcs" *Proc. Int. Workshop High Voltage Engineering 2014 (IWHV2014)*, ED-14-116, SP-14-072, HV-14-128 (2014)

[9] N. Shinsei, Y. Tanaka, Y. Uesugi, J. Wada, S. Okabe: "Numerical Simulation on Dynamics of Spallation Particles Ejected from Polyamide Materials during Irradiation of Ar Thermal Plasma", *International Conference on Electric Power Equipment - Switching Technology ICEPE-ST2011*, pp. 555-558 (2011)

[10] P. Rahimi, C.A.Ward: "Kinetics of Evaporation: Statistical Rate Theory Approach", *Int. J. Thermodynamics*, **8** (No.1), pp.1–14, (2005).

[11] Y. Tanaka, K. Kawasaki, T. Onchi, Y.Uesugi: "Numerical Investigation on Behaviour of Ablation Arcs Confined with Different Polymer Materials", *Proc.XVIIth Int. Conf. Gas Dischargees and Their Applications GD2008*, pp.161-164 (2008)

[12] Proulx P., Mostaghimi J., Boulos M.I.: "Plasma-particle interaction effects in induction plasma modelling under dence loading conditions", *Int. J. Heat Mass Transfer.*, Vol.28, No.7, pp. 1327-1336 (1985)

[13] Maher I. Boulos: "The inductively coupled R.F. (radio frequency) plasma", *Pure and Applied Chemistry.*, Vol.57, No.9, pp. 1321-1352 (1985)